

Critical currents in Josephson junctions with macroscopic defects

N. Stefanakis, N. Flytzanis

Department of Physics, University of Crete, P.O. Box 2208, GR-71003, Heraklion, Crete, Greece
(March 22, 2024)

The critical currents in Josephson junctions of conventional superconductors with macroscopic defects are calculated for different defect critical current densities as a function of the magnetic field. We also study the evolution of the different modes with the defect position, at zero external field. We study the stability of the solutions and derive simple arguments, that could help the defect characterization. In most cases a reentrant behavior is seen, where both a maximum and a minimum current exist.

I. INTRODUCTION

The interaction of localized magnetic flux (vortices) with defects (natural or artificial) or impurities in superconductors or junctions has an important effect in the properties of bulk superconductors or the behavior of Josephson junctions correspondingly [1]. The flux trapping from defects which is of importance in Josephson junctions [2] can modify the properties of polycrystalline materials with physical dislocations, for example grain boundary junctions [3]. In this category one can also consider grain boundary junctions in $\text{YBa}_2\text{Cu}_3\text{O}_{7-x}$ [4] where the tunneling current is a strongly varying function along the boundary. This strong inhomogeneity makes them good candidates for SQUID type structures [5]. Phenomenologically the current-voltage characteristics of grain boundary junctions are well described [6] by the resistively shunted junction model [7]. The grain boundary lines often tend to curve, while the junction is very inhomogeneous and contains nonsuperconducting impurities and facets of different length scales [8,9]. The linear increase of the critical current with length in grain boundary junctions with high- T_c superconductors, which is a different behavior from the saturation in the inline geometry of a perfect junction, can be explained by the presence of impurities [10]. Therefore it is interesting to study flux trapping in impurities especially when it can be controlled. Modern fabrication techniques can with relative ease engineer any defect configuration in an extremely controlled way.

In bulk materials are several types of defects that can influence the critical current in high temperature superconductors like $\text{YBa}_2\text{Cu}_3\text{O}_x$ materials. They include 3d inclusions, 2d grain boundaries and twin boundaries, and point defects like dopants substitutions, oxygen vacancies [1]. For example the homogeneous precipitation of fine Y_2BaCuO_5 non-superconducting particles in the melt processing of $\text{YBa}_2\text{Cu}_3\text{O}_x$ leads to high J_c values due to the particle pinning centers [11]. Similar behavior is observed in $\text{NdBa}_2\text{Cu}_3\text{O}_x$ bulk crystals with

$\text{NdBa}_2\text{Cu}_3\text{O}_{10}$ particles [12]. Of interest is also the case of the peak effect in twin-free Y123 with oxygen deficiency. In this case, one sees a linear increase (peak effect) of the critical current at small magnetic fields, when growth is under oxygen reduction [13]. For the fully oxidized crystal one expects a decrease. The peak effect is attributed to flux trapping. Information on the defect density and activation energies can also be obtained from the I-V characteristics, as was the case for several types of defects which were also compared to Au^+ irradiated samples with artificial columnar defects [14]. These columnar defects also act to trap flux lines in an YBCO film which is considered as a network of intergrain Josephson junctions modulated by the defects. In this case assuming a distribution of contact lengths one finds a plateau in the critical current density vs. the logarithm of the field [15].

The study of long size of impurities is going to give information beyond theories which concern small amplitude of inhomogeneities [16]. Also it is possible for a direct comparison of the numerical results with experiments in long junctions obtained with electron beam lithography [17]. This is a powerful technique which allows the preparation and control of arrays of pinning centers. Another method is the ionic irradiation which produces a particular kind of disordered arrays, consisting of nanosized columnar defects [14,18]. The variation of the critical current density can also occur due to temperature gradients [19].

The activity in the area of high critical current densities in the presence of a magnetic field is hampered by defects due to the difficulty of having a high quality junction with a very thin intermediate layer. Thus significant activity has been devoted, since for example the energy resolution of the SQUID [20] and the maximum operating frequency of the single flux quantum logic circuit [21], to name a few applications, depend inversely and directly respectively on the plasma frequency ω_p , with $\omega_p \propto J_c^{1/2}$. The fundamental response frequency of Josephson devices, the Josephson frequency ω_J , also depends on the critical current density. On the other

hand, a drawback is that high critical current densities lead to large subgap leakage currents [22] and junction characteristics degrade rapidly with increasing J_c .

Variations in the critical current density also influence the $I-V$ characteristics introducing steps under the influence of both a static bias current and the irradiation with microwaves [23]. In that case the variation is quite smooth (of sech type), so that the vorton and its motion could be described by a small number of collective coordinates. Interesting behavior is also seen in both the static and dynamic properties for the case of a spatially modulated J_c with the existence of "supersoliton" excitations [24,25] and the case of columnar defects [26,27] or disordered defects [10].

The trapping of vortices can be seen in the $I_{max}(H)$ curves where we also expect important hysteresis phenomena when scanning the external magnetic field. The hysteresis can be due to two reasons: (i) One is due to the non-monotonic relation between vortex and external magnetic field [28] arising from the induced internal currents, and (ii) from the trapping or detrapping of vortices by defects. The effect of a defect on a vortex and the strength of the depinning field depends strongly in the size of the defect, the type of defect and the position of the defect. Here we will consider case where the widths of the defects is of the order of the Josephson penetration depth. In this range we expect the strongest coupling between vortices and defects. We will also consider the case of a few defects in the low magnetic field region where pinning and coercive effects are important.

The organization of the paper is as follows. In Sec. 2 the sine-Gordon model for a Josephson junction is presented. In Sec. 3 we present the results of the critical current I_{max} versus the magnetic field of a junction with an asymmetrically positioned defect. The variation of the I_{max} and the vortex content N_f with the defect critical current density and the position are presented in sections 4 and 5 respectively. The effect of multiple pinning centers is examined in sections 6 and 7. In Sec. 8 we examine a defect with a smooth variation of the critical current density. In the last section we summarize our results.

II. THE JUNCTION GEOMETRY

The electrodynamics of a long Josephson junction is characterized from the phase difference $\phi(x)$ of the order parameter in the two superconducting regions. The spatial variation of $\phi(x)$ induces a local magnetic field given by the expression

$$H(x) = \frac{d\phi(x)}{dx} : \quad (1)$$

in units of $H_0 = \frac{\phi_0}{2d\lambda_J}$, where ϕ_0 is the quantum of flux, d is the magnetic thickness and λ_J is the Josephson penetration depth. The magnetic thickness is given by $d = 2\lambda_L + t$ where λ_L is the London penetration depth

in the two superconductors and t is the oxide layer thickness. The λ_J is also taken as the unit of length. The current transport across the junction is taken to be along the z direction. We describe a 1-D junction with width w (normalized to λ_J) in the y direction, small compared to unity. The normalized length in the x direction is x . The superconducting phase difference $\phi(x)$ across the defected junction is then the solution of the sine-Gordon equation

$$\frac{d^2\phi(x)}{dx^2} = J_c(x) \sin[\phi(x)]; \quad (2)$$

with the inline boundary condition

$$\frac{d\phi}{dx} \Big|_{x=\pm \frac{1}{2}} = \frac{I}{2} + H; \quad (3)$$

where I and H are the normalized bias current and external magnetic field. $J_c(x)$ is the local critical current density which is $J_c = 1$ in the homogeneous part of the junction and $J_c = j_d$ in the defect. Thus the spatially varying critical current density is normalized to its value in the undefected part of the junction J_0 and the λ_J used above is given by

$$\lambda_J = \frac{s}{2\mu_0 J_0};$$

where μ_0 is the free space magnetic permeability. One can also define a spatially dependent Josephson penetration depth by introducing $J_c(x)$ instead of J_0 . This is a more useful quantity in the case of weak distributed defects.

In the case of overlap boundary conditions Eqs. (2) and (3) are modified as

$$\frac{d^2\phi(x)}{dx^2} = J_c(x) \sin[\phi(x)] - I; \quad (4)$$

and

$$\frac{d\phi}{dx} \Big|_{x=\pm \frac{1}{2}} = H; \quad (5)$$

We can classify the different solutions obtained from Eq. (2) with their magnetic flux content

$$N_f = \frac{1}{2} (\phi_R - \phi_L); \quad (6)$$

in units of ϕ_0 , where $\phi_{R(L)}$ is the value of $\phi(x)$ at the right (left) edge of the junction. Knowing the magnetic flux one can also obtain the magnetization from

$$M = \frac{2}{\sqrt{\lambda_J}} N_f - H; \quad (7)$$

For the perfect junction, a quantity of interest is the critical magnetic field for flux penetration from the edges, denoted by H_{c1} . For a long junction it is equal to 2

while for a short it depends on the junction length. Due to the existence of the defect this value can be modified since we have the possibility of trapping at the defects. For a short junction we have penetration of the external

field in the junction length, so that the magnetization approaches zero. For a long junction it is a non-monotonic function of the external field H .

To check the stability we consider small perturbations $u(x;t) = v(x)e^{st}$ on the static solution $\phi(x)$, and linearize the time-dependent sine-Gordon equation to obtain:

$$\frac{d^2 v(x)}{dx^2} + \mathcal{P}_c(x) \cos(\phi(x)) v(x) = -s^2 v(x); \quad (8)$$

under the boundary conditions

$$\frac{dv(x)}{dx} \Big|_{x=0} = \frac{dv(x)}{dx} \Big|_{x=L} = 0;$$

where $s = \lambda^2$. It is seen that if the eigenvalue equation has a negative eigenvalue the static solution $\phi(x)$ is unstable. There is considerable eigenvalue crossing so that we must monitor several low eigenvalues. This is especially true near the onset of instabilities.

III. A SYMMETRIC DEFECT

In the following we will consider the variation of the maximum critical current as a function of the magnetic field for several defect structures. We start with a long ($L > \xi_J$) junction of normalized length $L = 10$ with a defect of length $d = 2$ which is placed $D = 1.4$ from the right edge. Thus the defect is of the order of ξ_J . We plot in Fig. 2a the maximum critical current I_{max} variation with the magnetic field. The different curves correspond to phase distributions for which we have a maximum current at a given value of the magnetic field H . The overlapping curves called modes have different ux content as seen in Fig. 2b where we plot the magnetic ux in units of ϕ_0 for zero current versus the external field. The magnetic ux is only a weak function of the external current.

For the perfect junction there is no overlap in the magnetic ux between the different modes. In fact each mode has ux content between $n\phi_0$ and $(n+1)\phi_0$ and therefore is labelled the $(n;n+1)$ mode [28]. Here in the case of the defect the range (at zero current) of ux for each mode can be quite different and the labelling is with a single index $n = 0;1;2;\dots$ corresponding in several cases to the $(0;1), (1;2), (2;3), \dots$ modes of the perfect junction. There are in several cases several modes with similar ux. To distinguish them we add a letter following the index n .

The maximum I_{max} is obtained for mode 1 and the increase comes from the trapping of ux by the defect. We have to note that the (d;e) part of this mode is a continuation of the (a;b) part of mode 0. In both cases we have entrance of ux from the no defect part of the

junction and the instability in the critical current occurs when $(\phi = 2) = \pi$. Here and in the following we will take this to mean equal to π modulo 2π . For the maximum current (at $H < 0$) the equation is $H = I = 2 = -2$. This can be understood from the pendulum phase diagram, where the $\phi = 2$ is the extremum slope, and thus the relation $I_{max} = 4 + 2H$ holds. For the (b;c) part of mode 0 the ux enters from the right where the defect is. This reduces the critical current compared to the perfect junction 0 mode [28,29]. Note that 0-mode has its critical current I_{max} peak slightly to the left of $H = 0$ in the I_{max} vs H diagram, and to the left of $N_f = 0$ in an I_{max} vs N_f diagram (see Fig. 11a). Also in the absence of current, reversing the direction of H only changes the sign of the slope $d\phi/dx$, but the phase difference (in absolute value) at the two ends will be the same. Thus the 0 mode at $I = 0$ extends for $-1.6 < H < 1.6$. This is not clearly seen due to curve overlapping in the left side. Comparing the I_{max} for the modes 1 and -1 we see that $I_{max}(1) > I_{max}(-1)$. In both cases a uxon (or anti-uxon) is trapped in the defect. The major difference in the I_{max} comes mainly from the phase distribution which in the mode 1 case leads to a large positive net current in the undefected side, while in the -1 mode the net current in the undefected side is very small.

For the mode 1, at $H = 0$ and zero current the instability happens due to the competition of the slope of the phase at the defect center and at the right edge, while at the other end at $H = 2$, the field at the defect center becomes equal to the external field applied at the boundaries and there is no such competition. In this case the instability sets in due to the critical value of the phase at the undefected boundary (i.e. $\phi(\phi=2) = 2$). The situation is analogous for the mode -1. For $H = 0$ the instability sets in due to the depinning of the anti-uxon while for $H = -2$ due to the critical value of the phase at the free defect part of the junction. For the mode 0 we have no uxon trapping at the defect, even though the instability at the two extremes with $H = \pm 1.6$ at zero current is caused from the tendency to trap a uxon or anti-uxon correspondingly at the defect. At higher values of the magnetic field ($|H| > 1.6$) we have stability for a range of non-vanishing current values as will be discussed below. Thus this value can be considered as the minimum value for the introduction of uxons in the junction. Let us remark that for the perfect junction, or a junction with a centered defect, the corresponding values for uxon introduction would be equal to 2. Thus there is a decrease of the critical field as the defect moves away from the center. For the 0 mode a centered defect would have no influence on the solution.

The results for the maximum current are in agreement with the stability analysis. In Fig. 2c we present the lowest eigenvalue λ_1 for the different modes in zero external current $I = 0$ as a function of the magnetic field H . The sudden change in slope for the modes -1;1 is because at that point a new eigenvalue becomes lower. The λ_1 is positive denoting stability and becomes zero at the criti-

cal value of the magnetic field, where a mode term inates. The symmetry about zero magnetic field is due to the symmetric boundary conditions for $I = 0$. Change of the sign of H changes the sign of the phase distribution, but the \cos in (8) remains unchanged. This symmetry is being lost when a finite current is also applied. Also there are solutions (not presented in the figure) for which the stability analysis gives negative eigenvalues i.e. instability. These solutions may be stabilized when we insert multiple impurities.

In Fig. 3a we specifically draw only the 1 mode, to be discussed in more detail. Here we changed the procedure, in searching for the maximum current. Up to now we followed the standard experimental procedure, i.e. we scan the magnetic field and for each value of H we increase the current I , starting from $I = 0$, until we reach the maximum current. Here we consider the possibility that for $I > 0$ there is also a lower bound in the value of the current for some values of the magnetic field. This requires a search where we vary both H and I simultaneously. Thus we see that for $H < 0$ there is a lower bound given approximately by the line $H + I = 2H_{c1}$, where $H_{c1} = 0$ is the critical value of H at $I = 0$, for which we have depinning of the trapped uxon. Over this curve the slope α_x at the right end (near defect) is kept constant and equal to H_{c1} and above this line the uxon remains pinned and it should be stable. This line ends at $H = -1$, since in that case the extremum value $\alpha_x = -2$ is reached in the left end. Increasing now in that range of H the bias current we find that also the I_{max} curve extends further to the left. The equation for this line is approximately given by $H + I = 2H_{c1}$, with an extremum at $\alpha_x (\alpha_x = -2) = -2$. Thus the instability on this line arises from the left side (far from the defect). It extends up to $H = -1$ for a long junction and joins the other line $H + I = 2H_{c1}$.

The above calculations were done for a long junction so that the fields at the two ends do not interfere. For shorter length however the two ends feel each other and in that case the two instabilities are not independent. This means that the tail of the defect free side field will compete with the slope of the trapped field. Then the two lines $H + I = 2H_{c1}$, and $H + I = 2H_{c2}$, end before they meet (at $H = -1$) at a critical magnetic field. Also for short junctions we expect the straight lines to have some curvature. A similar discussion holds for the right end of the 1 mode. Again there is a lower current (positive) bound given by $H + I = 2H_{c1}$ due to instability at the left end ($\alpha_x (\alpha_x = -2) = -2$), and an upper bound given by $H + I = 2H_{c2}$, where $H_{c2} = 2\beta$, due to uxon depinning. On the same diagram, we show the lower bound for negative currents. Thus we see that there is strong asymmetry for positive and negative currents. Remark that for negative currents the mode 1 is very similar to the mode (1,2) with no defect [28]. This is because the right boundary is determined by an instability at the undefected side. The left boundary is again very close because $H_{c1} = 0$. So an interesting effect of the defect

is that we have this strong asymmetry for positive and negative currents.

We would get a similar picture if we considered the 1 mode. In fact we get the same curves (as for mode 1) if we put $I \rightarrow -I$ and $H \rightarrow -H$. This is consistent with the 1 mode shown in Fig. 2a. The discussion can also be extended to the other modes. In Fig. 3b we show the result of a similar scan for the 0 mode, but for the sake of shortness we will not discuss the 1; 2; 2 modes. In any case when the number of uxons increases one must rely on numerical calculations rather than simple arguments.

IV. VARIATION WITH THE DEFECT CRITICAL CURRENT

In the previous section we considered the case of a microresistance defect. With present day masking techniques we can also consider any finite critical current (lower or higher) in the defect. This situation can also arise very often in junctions with high critical current densities, where small variations in the thickness can create strong critical current density variations. Thus for the previous asymmetric defect configurations we will study the effect of the defect critical current density in the magnetic interference pattern $I_{max}(H)$. We will concentrate on the 0 and 1 modes.

(i) mode 0:

In Fig. 4 we see the $I_{max}(H)$ variation for the mode 0 for decreasing values of the critical current density from $j_d = 2$, to $j_d = 0$. Let us discuss first the case for $j_d = 1$. For the perfect junction where $j_d = 1$ we have a symmetric distribution about $H = 0$. As we decrease j_d the ux content of this mode (and the extremum H) is symmetrically reduced (see Fig. 2b). It is not apparent from the drawing, due to the superposition of several curves on the left side of the diagram, but as expected the range of the magnetic field is symmetric about $H = 0$ at zero current. The corresponding $I_{max}(H)$ curves, however, are not symmetric. The right hand side of the curves is displaced towards smaller critical fields with decreasing j_d . This means that the critical field at $I = 0$ to introduce a uxon from the ends is decreased due to the existence of the defect which acts with an attractive force on the uxon. The curves are linear and can be approximated by the equation $I(H) = 4 - 2(H + H_c)$, where H_c is the decrease in the critical field H_{c0} and depends on j_d . A similar decrease happens for negative magnetic fields where the defect tries to pin an anti uxon. Even for higher currents the right side critical field is determined by the tendency of the defect to attract a uxon. The left hand side, however remains rigid (but is shifted along the line). This is due to the entrance of magnetic ux from that part of the junction where there is no defect. The instability in the critical current occurs when ($\alpha_x (\alpha_x = -2) = -2$) for every value of j_d . From the pendulum phase diagram which is the classical analog of the Josephson junction, the extremum occurs at $\theta_x (\alpha_x = -2)$, or

For $I=2$ which is the equation for this triangular side. At near zero current the critical field is influenced from the attractive action of the defect. At low currents and extreme negative magnetic field the I_{max} curve shows a re-entrance behavior so that it is not stable at low and high currents, but only for a finite intermediate range of current values. This way we reconcile the different origins of the instability mechanisms ($I=2$) = at high current and the defect influence discussed for the right hand side of the mode.

For $j_d > 1$ we see an increase in the I_{max} , while the critical magnetic field at $I = 0$ remains almost constant at about $H_{cr} = 1.9$. The instability at that point is due to the trapping of vortices in the region between the positive defect and the right edge of the junction. The field for that is expected to be near $H = 2$ if the right undefected part is of length of the order of Josephson length. Thus it is the same value for vortex penetration from the perfect junction edges. It will vary weakly with j_d .

(ii) mode 1:

The mode 1 in the perfect junction has a full vortex for magnetic field $H = 0.07$. The phase distribution is about $\phi = \pi$ where the energy has a minimum. At the end of this mode at $H = 2.07$ where two vortices have entered the junction the phase changes from $(\phi=2\pi) = \pi$ to $(\phi=2\pi) = 3\pi$. When the defect is inserted this mode is significantly modified due to the vortex trapping in the defect.

In Fig. 5 we see the magnetic interference pattern for this mode for different values of the defect critical current density. For $0 < j_d < 0.7$ the I_{max} vs H curves are displaced downwards, and a vortex is trapped in the defect. We notice that all the curves for $j_d < 0.7$ have the same critical magnetic field $H = 2$ for $I = 0$. This is because at this end of the mode, at $I = 0$ the instability arises at the side with no defect where the phase reaches the critical value $\phi = (\text{mod } 2\pi) = 0$. Of course as discussed in the previous section we have a reentrant behavior above $H = 2$. At the other end for small magnetic field the instability is due to depinning of the trapped vortex. For $0.7 < j_d < 1.0$ the defect can trap the vortex only for $H < H_{cd}$, where the value of the H_{cd} depends on the defect critical current j_d and in Fig. 5 it is shown for $j_d = 0.9$. Notice that for this value of j_d the vortex is very weakly trapped, and the untrapping process happens slowly over a range of magnetic field values. For $H > H_{cd}$ the vortex has moved away from the defect, and for this weak defect the junction does not feel it. The critical current goes abruptly close to the curve for the perfect junction. We conclude that the behavior of the junction for values of j_d close to $j_d = 1$ is determined by the ability of the defect to trap one vortex. This can be seen also from the change in the lowest eigenvalue variation with the external field H , at values of the critical density $j_d > 0.7$, in Fig. 6.

For $j_d > 1$ (thin lines in Fig. 5) it has a similar form as for $j_d = 1$, i.e. there is no vortex trapping. Again, as in the 0 mode, the H_{cr} at $I = 0$ stays around 2.0 and is

again due to the trapping of vortices in the right edge.

In Fig. 7 we present the evolution of I_{max} with the defect critical current density j_d for a magnetic field $H = 1.5$. For this value of the magnetic field there are no solutions with trapped vortices for $j_d > 0.83$. The lowest eigenvalue at $I = 0$ becomes zero at this point. For $j_d > 0.83$ and $H > 1.5$ there are solutions which are not trapped. For these solutions the maximum current coincides with the one of the perfect junction and there is a discontinuity in the curves. Notice the point at $j_d = 1.0$. In the same figure we also show the magnetic flux at $I = 0$ and at I_{max} which is almost constant as a function of j_d as expected, with small difference between the two different current curves.

V. VARIATION WITH THE DEFECT POSITION

In Fig. 8a we see the evolution of the critical current at zero magnetic field as we move the defect from the right edge of the junction $D = 0$ to the left edge where $D = 8$. The position is measured from the edge of the junction to the nearest edge of the defect. We examine the several modes separately:

(i) mode 0

For this mode and for $I = 0$, we are able to find solutions for all the defect positions. As we can see in Fig. 8b the corresponding magnetic flux at I_{max} is slowly changing and equal to zero when the defect is in the junction center. But when the defect is placed close to the ends the magnetic flux at the maximum current deviates from zero. The critical current for this mode is symmetric for defect positions about the junction center, and has its maximum value when the defect is at the center. This is because at that position it does not influence the solution at the edges which is very close to the undefected case, while near the center the phase is almost zero. But when the defect comes close to the junction ends the defect cuts into the area by which the current flows, and the critical current is reduced.

For even smaller distances $D = 0.2$, and $D = 0$ there is a jump to solutions which correspond to a current, which is much higher than that of the 0 mode for nearby D values. This is because the defect cuts negative current regions and for this position we have an increase of the critical current. In fact these solutions (see ++ symbols in Fig. 8a) are very close to the solutions of a perfect junction within the undefected area, except that now the defect at the edge can give contribution to the flux but no contribution to the current. Thus the flux is much higher than that of the 0 mode and it approaches that of mode 1. Nevertheless these points should be considered as a separate mode. In fact they are part of a branch (crosses). In these distances there are no other modes for $H = 0$. Similar results were obtained by Chow et al: [30] where they attributed this enhancement in the I_{max} for small distances to a self field which was generated by

the current, penetrating into the defect and resisted any further penetration of field. To overcome this resistance it was necessary to apply a higher current. But they do not distinguish between modes with different flux content, and their evolution with the defect position.

(ii) modes 1, -1

For these modes we do not have solutions for all the defect positions at $I = 0$ and $H = 0$, but only in the range $1.4 < D < 6.6$ as seen in Fig. 8c where the lowest eigenvalue is plotted as a function of the defect position for the different modes. The curves for the 1 and -1 modes coincide, while the 0 mode shows a change of slope corresponding to the last two points ($D = 0$ and 0.2 discussed above) which belong to another curve. Mode -1 has a trapped anti-uxon in the defect. When the defect is to the left ($4.0 < D < 6.5$), then the instability in the current of mode -1 at $H = 0$ is created at the right-end of the junction when the phase reaches the critical value

$(\theta = 2\pi)$. This instability occurs for currents which are less than those necessary to unpin the anti-uxon. Notice that increasing the current there is no competition with the slope of the anti-uxon trapped in the left end. Thus at this point (for $4.0 < D < 6.5$) the maximum current is very close to the undefected junction mode 0, except that in this case $N_{\text{eff}} = 1$ is close to an anti-uxon. At the other end ($D < 4.0$) the instability for mode -1 is caused by the depinning action of the applied current, which takes now much smaller values (close to zero) because of competition with the pinned uxon. The phase distribution at the defect free end is that expected for $H = 0$ and I close to zero. The mode 1 with a uxon trapped has a symmetrically reflected (about the center) form in I_{max} vs D and the instability for $D > 4.0$ occurs at the left end of the junction, which is the opposite case of mode -1. The eigenvalue becomes zero at the positions $D = 1.4$ and $D = 6.6$. The $\theta_1(D)$ curve coincides for the modes 1 and -1 due to the fact that the phase distributions for the same D for these modes are symmetric about $x = L/2$, and the $\cos(\theta)$ that enters the eigenvalue equation is the same.

In the rest we examine the variation of the critical value at which the instability sets in, as we scan the magnetic field in the positive (negative) direction H_{cr} (H_{cl}) for zero current, for the different modes, as a function of defect position. This instability can be attributed to the pinning, or the depinning field or to the critical value of $\frac{d}{dx}$ at the defect free edge, depending on the particular mode that we are considering. Explicitly for the mode 0 the instability in the H_{cl} (H_{cr}) is due to the pinning of a uxon (anti-uxon), respectively. In this mode the defect has no influence for positions close to the center as seen in Fig. 9a and 9b. However as we move the defect close to the edges the pinning field H_{cl} (H_{cr}) is reduced in absolute value because it is easier to trap a uxon (anti-uxon). For the mode 1 the H_{cr} is constant for all defect positions. This is due to the fact that at $I = 0$ it is the phase distribution at the undefected edge of the junction that determines the instability. Notice that due to the re-

trant character the critical magnetic field takes higher values at larger bias currents which vary with defect position. The H_{cl} curve depends on the phase distribution near the defect and therefore is strongly defect position dependent. For the mode -1 the picture is reversed compared with the 1 mode. In this case the H_{cl} is constant while the H_{cr} varies with position. Note that in this mode the depinning of an anti-uxon is the reason that causes the instability at H_{cr} .

V I. T W O S Y M M E T R I C P I N N I N G C E N T E R S

As noted defects (with $j_d < 1$) or inhomogeneities in the junction can play the role of pinning centers for a uxon. In this section we discuss more precisely the effect of multiple pinning centers on the magnetic interference patterns $I_{\text{max}}(H)$ and the flux distribution. The pinning effect of the Josephson junction has also been analyzed in [31,32], by using a simple mechanical analog. The analogies of the mixed state of type II superconductors and vortex state of the Josephson junction has been discussed in these references. In Fig 10a we present, as an example, the critical current I_{max} versus the magnetic field for a junction which contains two defects of length $d = 2$ placed symmetrically at a distance $D = 2$ from the junction's edges. We examine the following modes grouped according to flux content:

(i) modes 0, 0a

These modes have magnetic flux antisymmetric around zero field, as seen from Fig. 10b where the magnetic flux is plotted versus the magnetic field. At $I = 0$ and magnetic field $H = 0.7$, the 0a mode contains one uxon trapped in the left defect, while an anti-uxon exists at the other part of the junction. As H increases towards 0.7 the picture changes slowly, so that the anti-uxon is pinned in the right defect. The stability analysis shows that this mode is unstable. We remark that there are also other unstable modes near zero flux, which we will not present here. For example there is another unstable mode with the same flux as 0a but a much higher critical current (the same as the 0 mode). Mode 0 has phase distributions which are similar to the corresponding mode of the homogeneous junction since it has no trapped flux in each defect.

(ii) modes 1l, 1r

These modes have magnetic flux close to unity, and are both stable. For the mode 1r one uxon has been trapped to the right defect, and in the mode 1l, the vortex is trapped in the left defect. Due to the symmetry this mode has the same magnetization as the mode 1r, but the critical current is reduced. The phase distribution for the modes 1r, and 1l, at zero current are related by $\theta_{1l}(x) = 2\pi - \theta_{1r}(x)$. The maximum field $H = 1.9$ (at $I = 0$) for both modes is determined by an instability at the defect free side. At the other extreme there is a competition at the uxon side between the applied

eld and the eld created by the pinned uxon. Thus the critical eld at $H = 0.62$ can be considered as a coercive eld and below this value the uxon gets unpinned. The two modes have characteristically different currents and this depends on the current through the uxon free defect, since the pinned uxon itself gives no major contribution. Thus the maximum current is much larger for the 1r mode. The opposite would be true if we look for negative currents. There are also the symmetrically situated modes that correspond to an anti uxon in the left or right defect, which are not shown in Fig. 10a. The respective flux is antisymmetric with H around $H = 0$.

In Fig. 10a we also show the mode 2 with flux around 2 uxons. Several unstable modes are not shown, for the sake of clarity. Their analysis however, can show the connection between different modes, while a defect in the correct place with proper characteristics can stabilize these solutions. We conclude that depending on the positions where the vortex is trapped we may have modes with the same magnetic flux content, but different critical currents. Also due to soliton localization on the defects, we may have stable states with magnetic flux close to unity, for zero magnetic eld. These states together with the one existing in the homogeneous junction form a collection of stable states in a large H interval. We must comment here that states with unit flux, for zero magnetic eld ($H = 0$) exist in the homogeneous junction, as a continuation of the stable (1) mode to negative magnetic elds, but as we found in a previous work [28], are unstable. So we may argue here that the presence of defects stabilizes these states.

In comparing the results for one (Fig. 2a) and two defects (Fig. 10a) we see some similarities and differences. In the case of two defects new modes appear but also the region of stability of the equivalent modes is different. This is more clearly seen in Fig. 11 where we plot the I_{max} vs N_f for both cases. This presentation is useful since the N_f is a nonlinear function of H . This plot (Fig. 11a) is a combination of Figs. 2a and 2b. We should point out that the maximum peak in the current in both cases comes due to the trapping of a uxon in the defect at the right side. The maximum of 0-mode is very close in both cases and this happens because this mode does not involve uxon trapping. The 1r mode for the two defect case is very close to the 1 mode of the single defect, since in both cases there is a uxon trapped in the same side. In the two defect case we see an enlargement of the region of stability so that the modes overlap. The thin continuation lines in modes 0 and 1 for the single defect are in the reentrant region of flux as discussed in section 2.

VII. SYMMETRIC DISTRIBUTION OF PINNING CENTERS

In this section we study as an example the case where a junction of length $\ell = 14.2$ contains three defects of

length $d = 2$, and the distance between them is 2. The length was augmented, so that we keep the same width of the defects when we increase the number of the defects, since we saw that the width of the order $d = 2$, gives the possibility of uxon trapping and increased maximum current when the defect is situated asymmetrically. We will study the phase distribution at $I = 0$ and try to extract information about the critical eld values and magnetization. We end the following modes grouped according to flux content:

i) modes 0, 0l, 0r, 0c

In Fig. 12a we present the critical current versus the magnetic eld for the modes with magnetic flux around zero (see Fig. 12d). This is indicated by the 0 symbol. There are four modes belonging in this category, which are stable. The solutions for the mode 0 are similar to the homogeneous junction mode 0, with no flux trapping in the defects. The only difference is that the instability in the critical eld occurs when the phase at one edge, reaches a value, which is smaller (due to pinning) than the corresponding value for the undefected junction, which is $(\phi = 2) < \pi$. The same was true for the two defect case. Mode 0c has the maximum critical current $I_{max} = 5.08$ for $H = 0$. One anti uxon is trapped to the leftmost defect, one uxon to the rightmost, and the phase in the center defect is constant. The trapping at the edge defects leads to a positive current distribution between them, for this particular length, and enlarges the maximum current. The same type of mode was not found for the two defect case (with a shorter junction length), and we conclude that the extra defect along with the increased junction length stabilizes this solution. For the mode 0l one uxon is trapped in the left defect where the phase changes about the value $\phi = \pi$. The anti uxon is distributed at the other two defects, where the phase is about the values $3\pi/2$ (or $\pi/2$), and we have a cancellation of the positive and negative current density in this region. Similar for the mode 0r the uxon is trapped to the right defect, and the current is distributed with opposite sign to the other two defects. These modes are similar to the 0a mode for the two defect case.

ii) modes 1l, 1c, 1r

In Fig. 12b we see the maximum current versus the magnetic eld for the modes with magnetic flux around $N_f = 1$ (see Fig. 12e). There are three modes with flux close to $N_f = 1$ each of which corresponds to the trapping of one uxon in one defect. In the mode 1c the uxon is trapped in the center defect. In the mode 1l (1r) it has been trapped in left (right) defect. Due to the symmetry the lowest eigenvalue, and the magnetic flux coincides for these two modes, but as we showed in the previous section, their critical currents are different, depending on the tunneling current distribution in the region with no trapping. The 1r mode corresponds to a higher critical current.

iii) modes 2, 2a, 2b

In Fig. 12c we see the maximum current versus the magnetic eld for the modes with magnetic flux around

$N_f = 2$ (see Fig. 12f). Only the mode 2 corresponds to stable solutions. There we have two vortices trapped in the side defects. In mode 2a one vortex is trapped in the right defect, while in mode 2b this trapping occurs in the center defect. We conclude that distributed pinning centers are more effective in trapping the vortex, and lead to an increased critical current. Some conclusions will continue to be valid for larger number of defects where we keep the defect width and separation fixed. In that case we also expect the results to change significantly when there is either a periodic array of defects, where we expect higher vortex modes to give the highest current peak [26].

VIII. DEFECT WITH A SMOOTH VARIATION OF CURRENT DENSITY

Up to now we considered defects with abrupt changes in the local critical current density and the question arises whether the abruptness of J_c variation is crucial in the significant change in I_{max} for the $n = 1$ mode. We will see that similar effects exist for smooth variation, where again the vortex pinning is an important feature. For this reason we chose a single defect at the junction center with a smoothly varying critical current density given by

$$J_c(x) = \tanh^2 \frac{2}{\ell} (x - x_0) ; \quad (9)$$

where the defect is centered at x_0 , and the width is determined by ℓ . In Fig. 13 we show the results for the case $x_0 = 7.6$ and $\ell = 2$, which can be compared with the results of the asymmetric defect in Fig. 2a. For the modes shown the curves are very similar and thus we see that the main results survive since the defect strengths are similar. Of course there is a quantitative difference. But most of the stability criteria described earlier are still valid.

In Fig. 14 we consider the effect of the form of current input and compare the case of inline with overlap for a smooth defect situated at the center of the junction i.e. $x_0 = 0$ with $\ell = 0.5$. In Fig. 14a we present the I_{max} for inline boundary conditions, and we show only the $1;0;1$ modes. The 0 mode is not influenced at all from the defect since all the phase variation is at the boundaries. There is a strong similarity with I_{max} for the 1, and -1 modes. The reason is that in these cases there is a trapped vortex or anti-vortex at the center and at zero current and magnetic field the phase variation dies out at the boundaries. Thus when increasing the current at $H = 0$ towards I_{max} we have the same situation at the boundaries as for the 0 mode and the instability happens at close I_{max} values. Of course due to the pinning, the vortex content is very different from the 0 mode. The 1 and -1 modes have an enhanced I_{max} and the small difference in I_{max} from the 0 mode is attributed to the small influence of the trapped vortex to the boundaries.

Let us remark that a similar situation was seen in Fig. 8a for the square well defect, when the defect position is at the center for $H = 0$. By comparing with Fig. 9 the H_{c1} and H_{cr} values we see close agreement with the case of $j_d = 0$ in the defect. These results could change for a smaller length junction or if we move the defect towards the edges (as seen in Fig. 8a).

For the same defect we also investigated the effect of the overlap current input, where the current is distributed along the whole junction. In Fig. 14(b) we present the maximum current per unit junction length versus the magnetic field, and it should be compared to the inline case in Fig. 14(a). We see a significant change for the 1 and -1 modes. Of course at $I = 0$ both current inputs give the same solutions, but I_{max} is much smaller for the overlap boundary conditions. This is from the fact that due to the applied current the vortex is pushed against the pinning barrier until it is overcome at the critical current. In the absence of applied current the phase at the defect center is $\psi(0) = 0$, while the application of the current pushes the vortex to the edge of the defect which is taken to be near the point where the curvature of the defect critical current distribution changes sign. So we can consider in this case this maximum current as a measure of the pinning force.

In Fig. 15a we plot the magnetic flux N_f at zero current versus the magnetic field H for the inline case. The lowest eigenvalues for the different modes versus the magnetic field are seen in Fig. 15b. For a homogeneous junction the 0 mode is the only stable state available at $H = 0$. However in the problem we consider here, the mode $1(-1)$ exists and it is stable for $H = 0$ and corresponds to the localization of the soliton (antisoliton) in the inhomogeneity. For these modes we have pinned flux at $H = 0$, with $\psi(0) = 0$, and $\frac{d\psi}{dx} = 2$. In Fig. 16 we show the evolution of ψ and $\frac{d\psi}{dx}$, for the mode 1, as we change the magnetic field at $I = 0$. Near $H = 1.9$ the vortex content is near zero and for $H < 1.9$ an instability sets in due to the depinning of the vortex. This is because the slope at the pinned vortex competes with the opposite slope tried to be imposed by the external negative magnetic field at the boundaries. At the other end the flux is equal to 2, and the instability sets in when at the boundaries approaches $\pm\pi$ (or odd multiples). The range of H values for the 1 mode, when the defect is at the center is significantly broadened and gives a corresponding range for the flux of two vortices. Usually each mode has about one extra vortex and in particular for the perfect junction it contains only one extra vortex. This is because the defect is at the center and far enough from the edges where the magnetic field is applied and therefore even for negative fields there is no significant competition, with the field at the defect center. This is especially true when the distance of the defect from the edges is greater than $2\ell_J$. When however the defect is near the edge the instability sets in before we cross to negative magnetic fields.

The maximum current I_{max} for the mode 0 is greater than in the modes 1, 1, but is reduced compared with the I_{max} for the mode 0 in the homogeneous junction, in zero field. In [33] they approximated this reduction in an analytical calculation using a delta function for the defect potential, and they found $I_{max} = 0.02$. In [33] they arrived at the analytical result, by minimizing the vortex free energy, for the maximum overlap current versus the magnetic field H , for these modes, which is a good approximation of the numerical solution we consider here in the limit $L \rightarrow 1$.

IX. CONCLUSIONS

In several applications it is desirable to work in an extremum of the current for a region of the magnetic field. This can be achieved by the appropriate distribution of defects so that the negative lobes of the current distribution in the junction due to the vortices are trapped in the defect with no contribution to the current. Of course if the defect is isolated (far from other defects or the edges) we expect zero contribution to the current. Due to the effect of the applied current and magnetic field at the boundaries in certain cases we can obtain positive current lobes outside the defect. In several cases in section 3 this was the reason for the increased current. Because the control of magnetic field is very easy compared to other system parameters (like temperature, disorder, etc.) the measurement of the effect of magnetic field on junction behavior, provides a convenient probe for the junction. The calculation of the I_{max} can characterize the quality of the junction or verify the assumed distribution of defects when they are artificially produced. The spatial variation of the critical current density in low T_c -layered junctions, and high T_c grain boundary junctions can be directly imaged with a spatial resolution of 1 μm using low temperature scanning electron microscopy (LTSEM) [34,35]. Information on smaller scale inhomogeneities has to rely on the magnetic field dependence of the maximum tunneling current I_{max} .

The purpose of this paper is the consideration of large defects in order to study the interaction between vortices and defects and give estimates of the coercive field for pinning or depinning of a vortex from a defect. The region of consideration puts us far from the region of perturbation calculations and is amenable to direct experimental verification since it is easy to design a junction with the above characteristics. The defects influence strongly the low vortex modes. At high magnetic fields larger than the depinning field of a single vortex we expect only minor effect and vortex trapping. Of course for a large number of defects interesting behavior can be obtained. [24,25] The interaction between vortices in the few defect case also assists to overcome coercive fields and untrap vortices. The results of two trapped vortices in the two defect case show that the vortices are strongly

coupled and one cannot consider an exponential interaction type potential between the vortices. Also the critical current in a long junction, cannot be calculated as the Fourier transform of the spatial distribution of the critical current density $J_c(x)$, at least for weak magnetic fields. For strong magnetic fields, where we have the field penetrating uniformly the junction, as is the case for short junctions, we recover the diffraction like pattern.

In summary we saw that the bounds of the different modes determined by the stability analysis depend on two factors: (i) the instability at the boundaries away from the defect when x reaches its extremal values equal to ± 2 , and (ii) the instability due to the pinning or depinning of a vortex by the defect. If the junction is near one end then we saw that both criteria play a role in determining the instability, independently in different areas. In general, however, there will be coupling between defects and the edges (surface defects) especially in the case of multiple defects. Defects also introduce hysteresis phenomena which are weaker in the case of smooth defects. We also saw that due to vortex trapping in general we see a reentrant behavior, i.e. there are regions of magnetic field for which there is both an upper and a lower bound on the maximum current. We also found that due to the pinning of magnetic vortex from the defect there exist additional stable states in a large interval of the magnetic field. The abrupt change in the critical current density is not crucial for the trapping. Similar results are expected from smooth defects, with quantitative differences. The above results can be checked experimentally since it is easy to design a junction with a particular defect structure, using masking techniques. In fact a few parameters or characteristics could give at least partial information on defect properties. In particular the measurement of H_{cr} or H_{cl} can give some information of the defects near the edges. Also one can imagine the situation where we scan locally with an electron beam affecting thus the local critical current and observe the variation of the I_{max} as we increase the heating. Once a vortex is trapped we can decrease the heating (or increase j_d) and observe the variation of I_{max} . Thus one can have pieces of information to put together in guessing the defect structure that might fit the whole I_{max} pattern. The extension to many defects requires considerable numerical work. It is hoped, however, that some of the stability criteria will still be useful.

Acknowledgements One of us (N.S.) would like to acknowledge the ESF/FERLIN programme for partial support. Part of this work was done under grant PENED 2028 of the Greek Secretariat for Science and Research.

[1] See several papers in the Conference Proceedings on Vortex Matter in Superconductors at Extreme Scales and

- Conditions, Eds. V. V. Molshchakov, P. H. Kes, E. H. Brandt in *Physica C* 332, Nos. 1-4, May (2000).
- [2] A. Barone, and G. Paterno, *Physics and Applications of the Josephson Effect* (Wiley, New York, 1982).
- [3] D. Dimos, P. Chaudhari, and J. Mannhart, *Phys. Rev. B* 41, 4038 (1995).
- [4] E. Samelli, P. Chaudhari, and J. Lacey, *Appl. Phys. Lett.* 62, 777 (1993).
- [5] R. Gross, P. Chaudhari, M. Kawasaki, M. B. Ketchen, and A. Gupta, *Phys. Rev. Lett.* 57, 727 (1990).
- [6] R. Gross, P. Chaudhari, D. Dimos, A. Gupta, and G. Kozen, *Phys. Rev. Lett.* 64, 228 (1990).
- [7] D. E. Mcumber, *J. Appl. Phys.* 39, 3113 (1968).
- [8] D. J. Miller, H. Talvacchio, D. B. Buchholz, R. P. H. Chang, *Appl. Phys. Lett.* 66, 2561 (1995).
- [9] J. Ayache, A. Torel, J. Lesieur, U. Dahmen, *J. Appl. Phys.* 84 4921 (1998).
- [10] R. Fehrenbacher, V. B. Geshkenbein and G. Blatter, *Phys. Rev. B* 45, 5450 (1992).
- [11] T. Oka, Y. Itoh, Y. Yanagi, H. Tanaka, S. Takashima, Y. Yamada and U. Mizutani, *Physica C* 200, 55 (1992).
- [12] A. Takagi, T. Yamazaki, T. Oka, Y. Yanagi, Y. Itoh, M. Yoshikawa, Y. Yamada and U. Mizutani, *Physica C* 250, 222 (1995).
- [13] Th. Wolf, A.-C. Bomarel, H. Kupfer, R. Meier-Himer, and B. Obst, *Phys. Rev. B* 56, 6308 (1997).
- [14] C. Camerlingo, C. Nappi, M. Russo, G. Testa, E. Mezzetti, R. Gerbaldi, G. Ghigo and L. Gozzelino, *Physica C* 332, 93 (2000).
- [15] E. Mezzetti, A. Chiodoni, R. Gerbaldi, G. Ghigo, L. Gozzelino, B. Minetti, C. Camerlingo and A. Monaco, *Physica* 332, 115 (2000).
- [16] M. V. Irokov, and A. E. Koshelev, *JETP* 70, 547 (1990).
- [17] K. K. Roger, L. N. Smith, and D. W. Jllie, *Appl. Phys. Lett.* 39, 280 (1981).
- [18] C. J. van der Beek, M. Konczykowski, R. J. Drost, P. H. Kes, A. V. Samoilov, N. Chikumoto, S. Bourdard, M. V. Feigel'man, *Physica C* 332, 178 (2000).
- [19] V. M. Krasnov, V. A. Bozhnov and N. F. Pedersen, *Phys. Rev. B* 55, 14486 (1997).
- [20] M. B. Ketchen, *IEEE Trans. Magnetics* 27, 2916 (1991).
- [21] K. K. Likharev and V. K. Semenov, *IEEE Trans. Appl. Supercond.* 1, 3 (1991).
- [22] A. W. Kleinsasser, W. H. Mallison, R. E. Miller and G. B. Arnold, *IEEE Trans. Appl. Supercond.* 5, 2735 (1995).
- [23] G. Reinisch, J. C. Fernandez, N. Flytzanis, M. Taki and S. Pnevmatikos, *Phys. Rev. B* 38, 11284 (1988).
- [24] V. A. Bozhnov and A. V. Ustinov, *Phys. Lett. A* 139, 481 (1989).
- [25] B. H. Larsen, J. Mygind and A. V. Ustinov, *Phys. Letters A* 193, 359 (1994).
- [26] M. A. Itzler and M. Tinkham, *Phys. Rev. B* 51, 435 (1995).
- [27] L. Balents and S. H. Simon, *Phys. Rev. B* 51, 6515 (1995).
- [28] J.-G. Caputo, N. Flytzanis, Y. Gaididei, N. Stefanakis, and E. Vavalis, *Supercond. Sci. Technol.* 13, 423 (2000).
- [29] C. S. Owen, D. J. Scalapino, *Phys. Rev.* 164, 538 (1967).
- [30] T. C. Chow, H. Chou, H. G. Lai, C. C. Liu, Y. S. Gou, *Physica C* 245, 143 (1995).
- [31] T. Yamashita, L. Rinderer, K. Nakajima, and Y. Onodera *J. Low Temp. Phys.* 17, 191 (1974).
- [32] T. Yamashita, and L. Rinderer, *J. Low Temp. Phys.* 21, 153 (1975).
- [33] A. T. Filippov, Yu. S. Gal'perin, T. L. Boyadjev, and I. V. Puzynin, *Phys. Lett. A* 120, 47 (1987). 21, 153 (1975).
- [34] R. P. Huebener, *Adv. Electron. Elect. Phys.* 70, 1 (1988).
- [35] R. Gerdenann, K. D. Husemann, R. Gross, L. Al, A. Beck, B. Elia, W. Reuter and M. Siegel, *J. Appl. Phys.* 76, 8005 (1994).

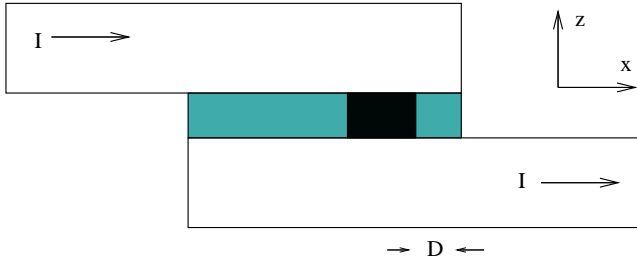


FIG. 1. The geometry of the junction. The dark shaded region marks the defect in the intermediate layer. L is the junction length and D the separation between the left edges of the defect and the junction.

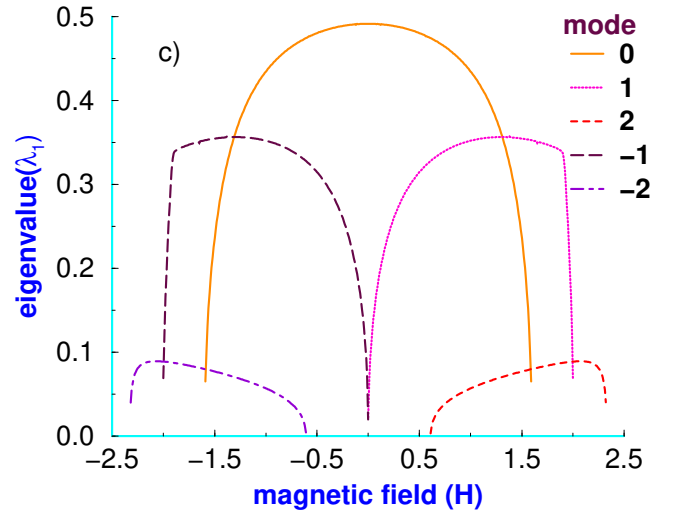
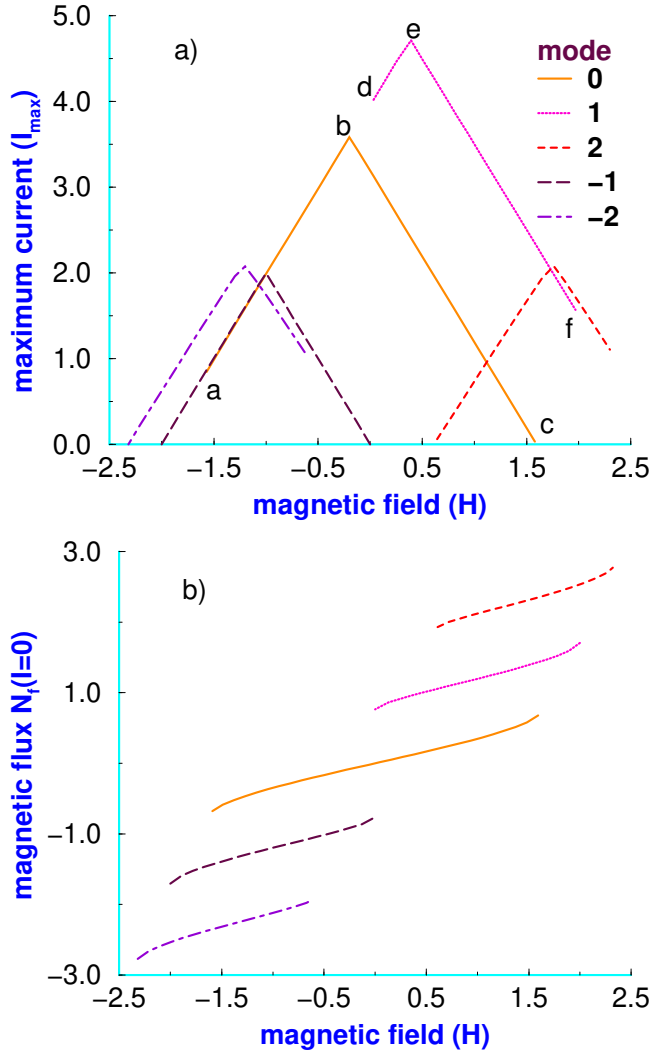
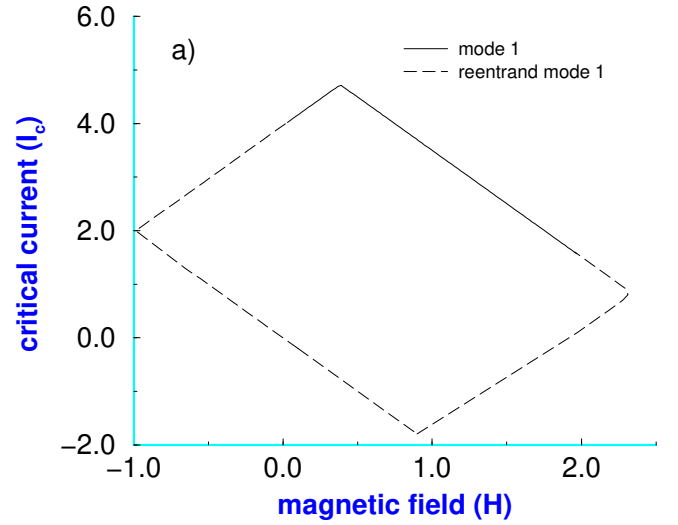


FIG. 2. (a) Critical current I_{\max} and (b) magnetic flux at zero current, versus the magnetic field H , for the different modes. $L = 10$ and $D = 1.4$. (c) The evolution of the lowest eigenvalue λ_1 with the external field for the different modes. At the extremes of each mode λ_1 vanishes.



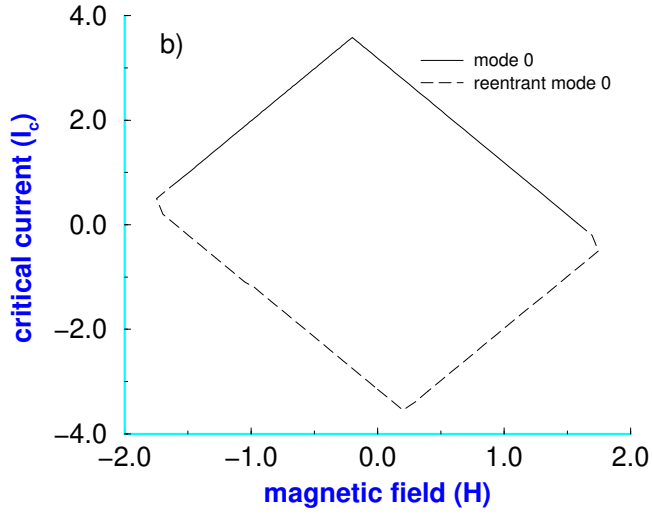


FIG .3. (a) Critical values of the bias current as a function of the magnetic field. The solid line is drawn for the mode 1 obtained with the usual procedure starting from zero current and increasing the current to the critical value, while the dashed line represents the values obtained with the reentrant procedure described in the text. (b) The same information as in (a), but for the mode 0.

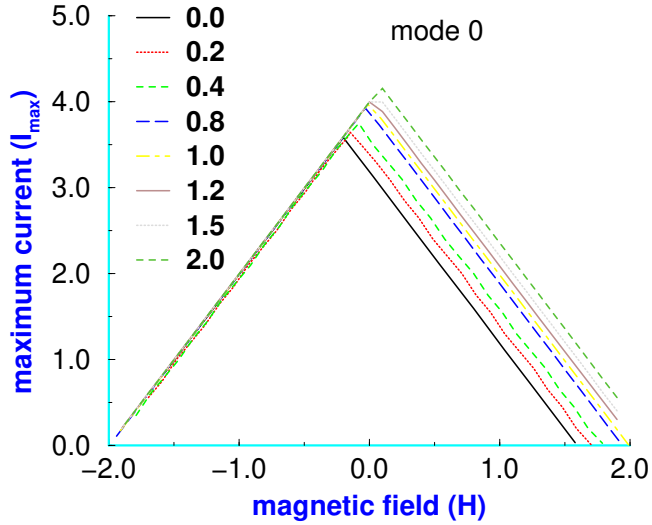


FIG .4. Critical current as a function of the magnetic field, for the mode 0, for different values of the defect critical current density j_d .

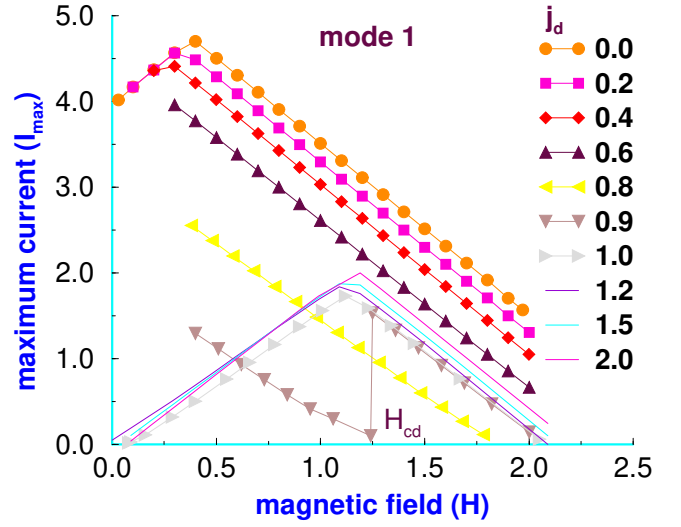


FIG .5. Same as in Fig. 4, but for the mode 1.

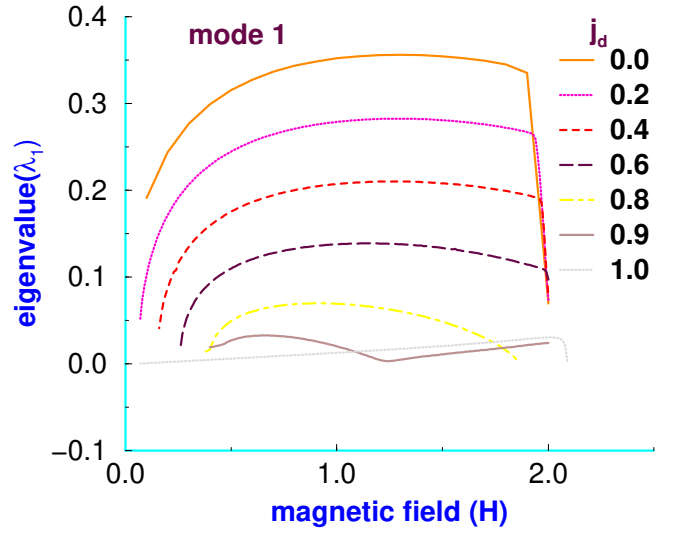


FIG .6. The lowest eigenvalue versus the magnetic field for the mode 1 for different values of the defect critical current density j_d .

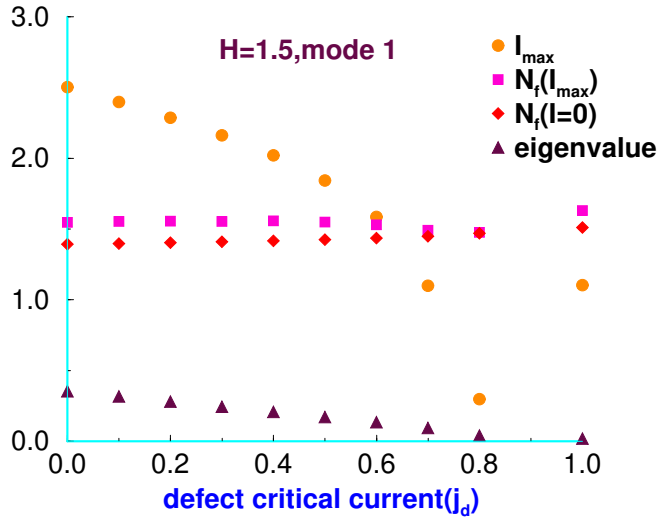


FIG. 7. Critical current versus the defect critical current density j_d , for magnetic field equal to $H = 1.5$, for the mode 1. In the same graph the magnetic flux at zero and maximum current, and the lowest eigenvalue at $I = 0$ are plotted as a function of the j_d .

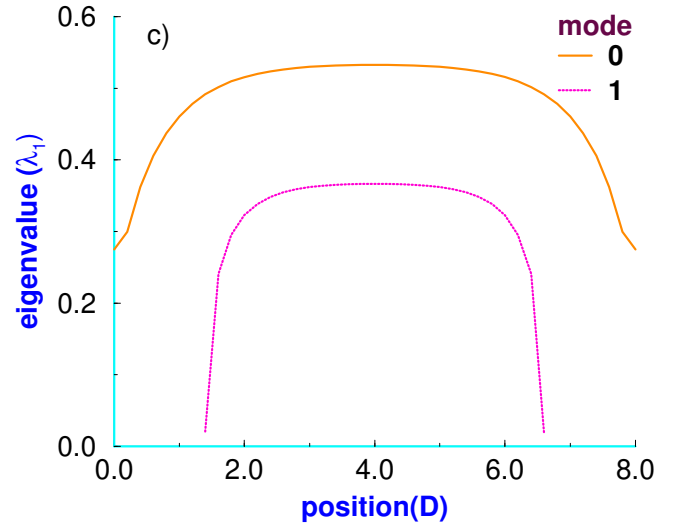
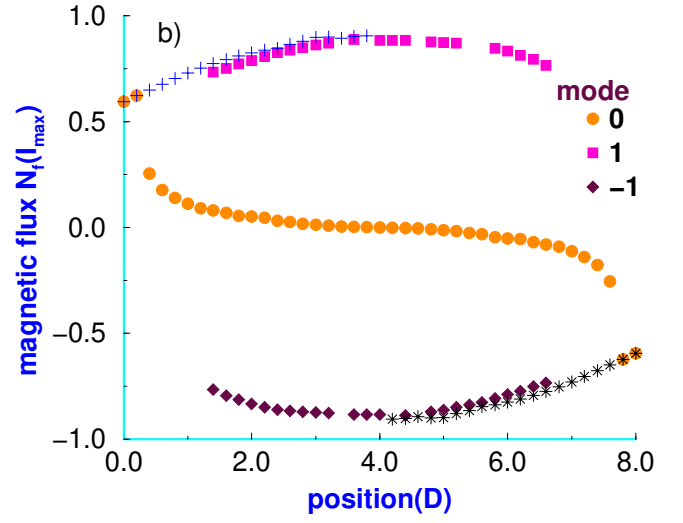
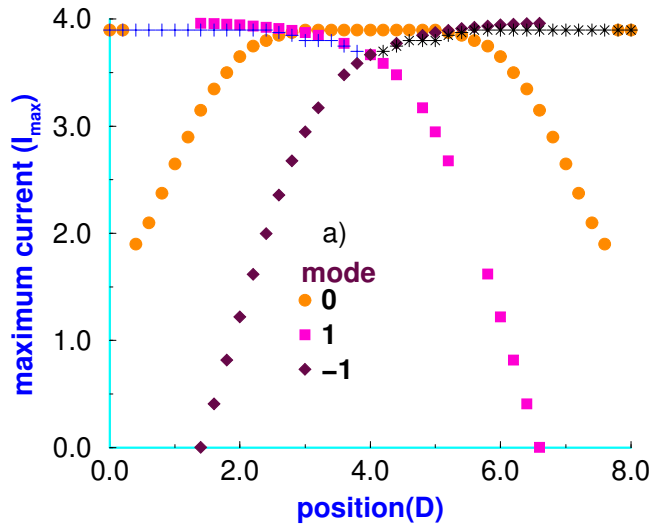


FIG. 8. The variation of (a) the maximum current I_{max} and (b) the magnetic flux N_f at the maximum current, versus the defect position D , measured from the right edge of the junction, for the modes 0, 1, -1. The crosses and stars lines are continuations of the two points at the two ends of the graph. (c) the corresponding lowest eigenvalue at zero current versus the defect position D , for the modes 0, 1. The -1 mode eigenvalue is the same as for the 1 mode.

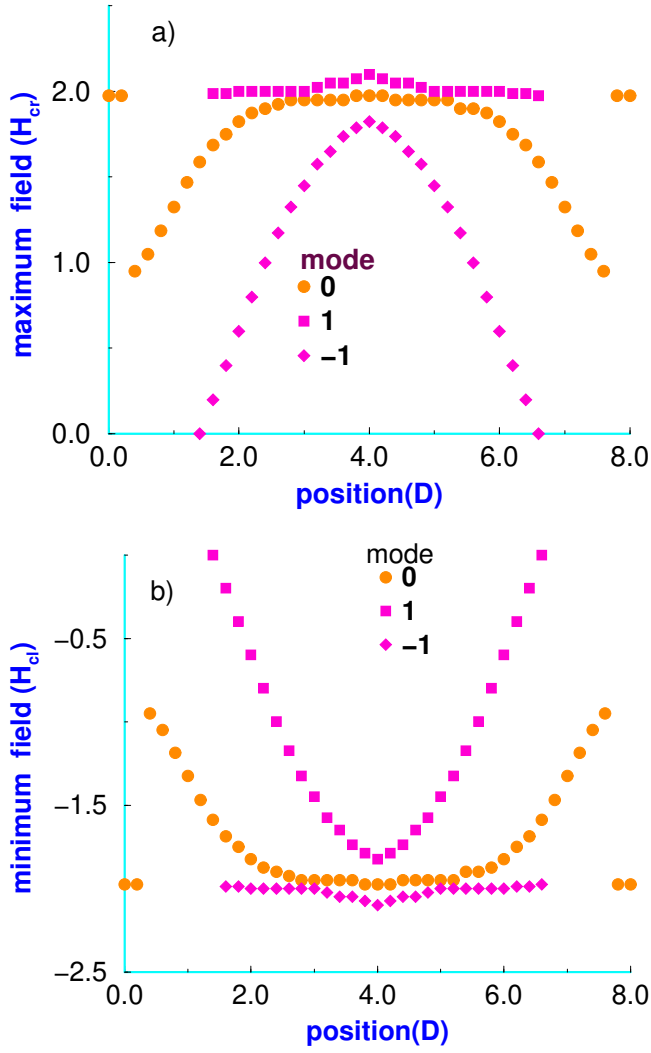


FIG .9. (a) The critical value of instability as we scan the magnetic field to the right H_{cr} as a function of the defect position D , for the modes 0, 1, -1. (b) The same as (a) but to the left for the H_{cl} .

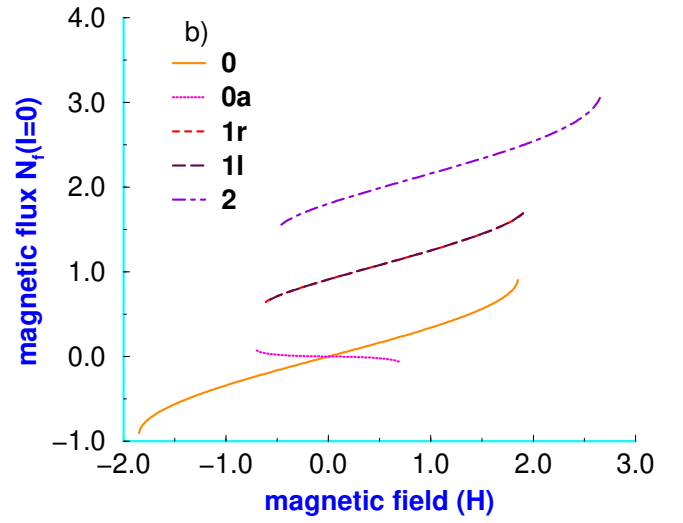
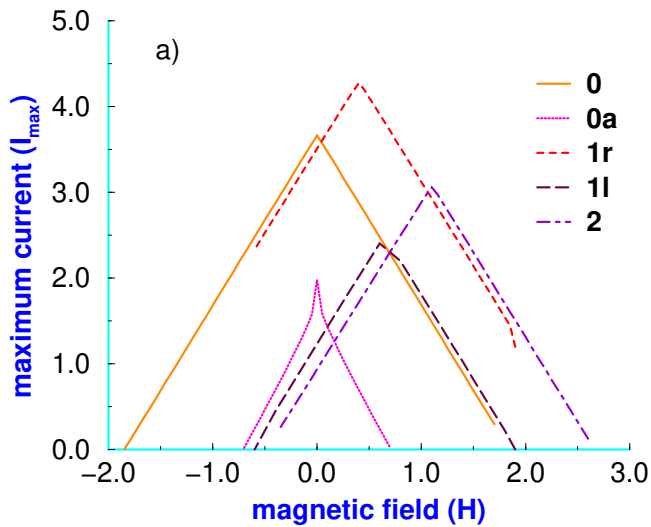


FIG .10. (a) Critical current I_{max} and (b) magnetic flux N_f , versus the magnetic field H , for the different modes, for a junction of length $\ell = 10$, which contains two symmetric pinning centers of length $d = 2$.

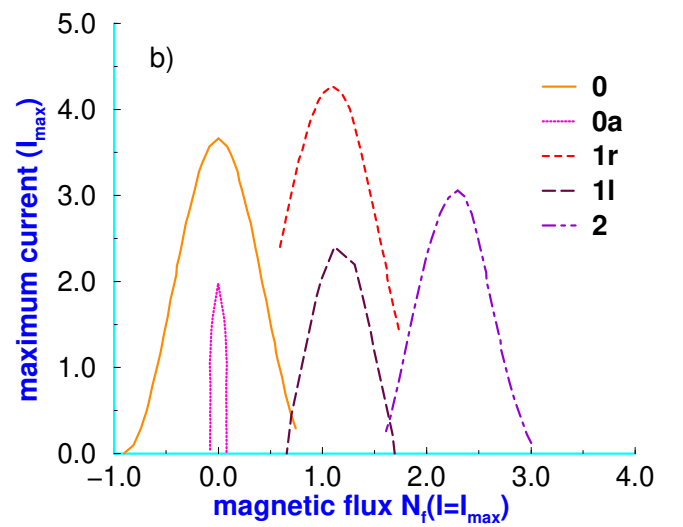
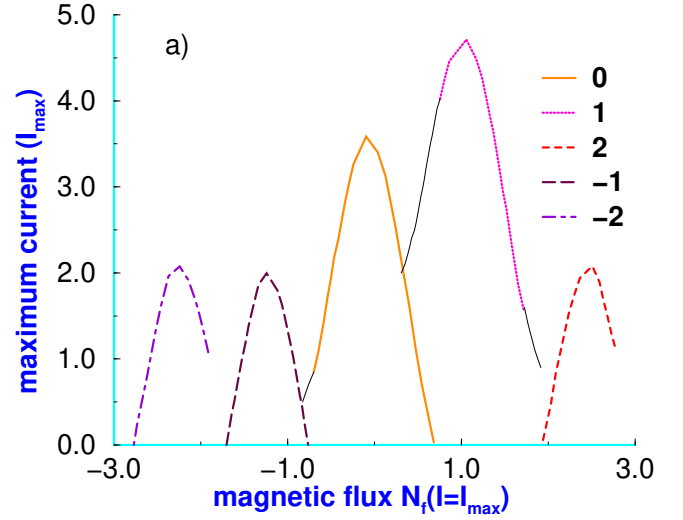
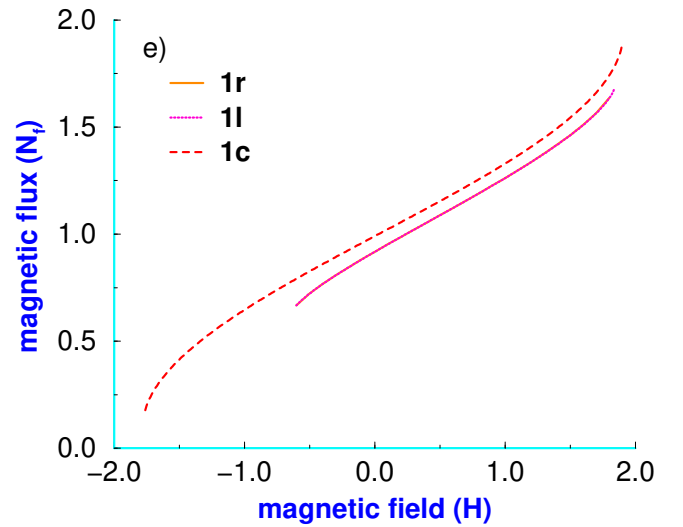
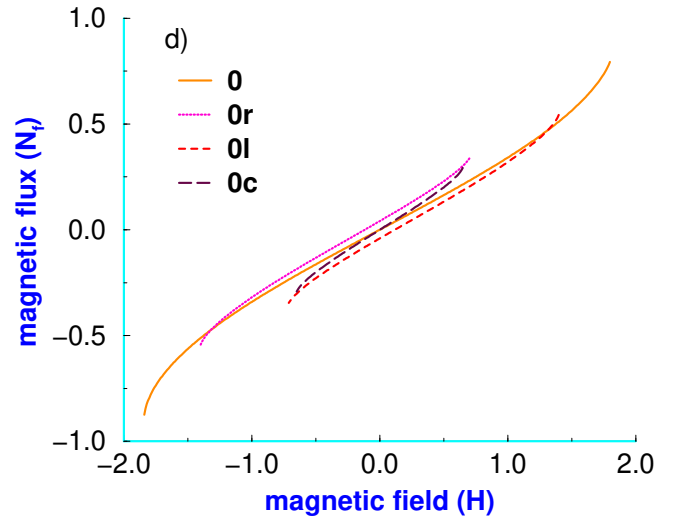
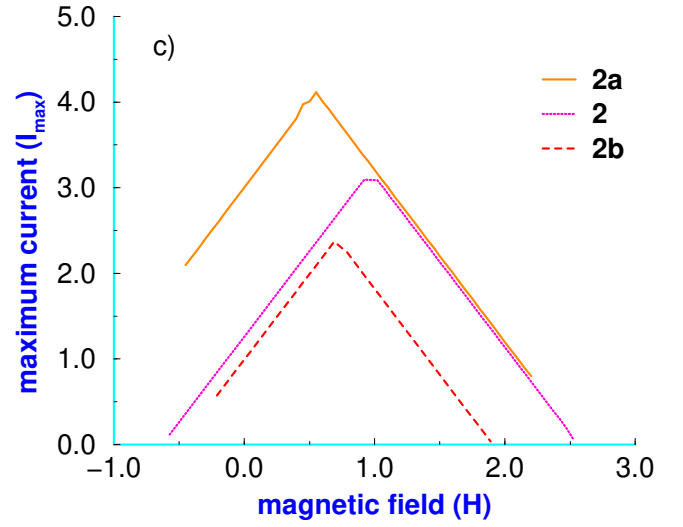
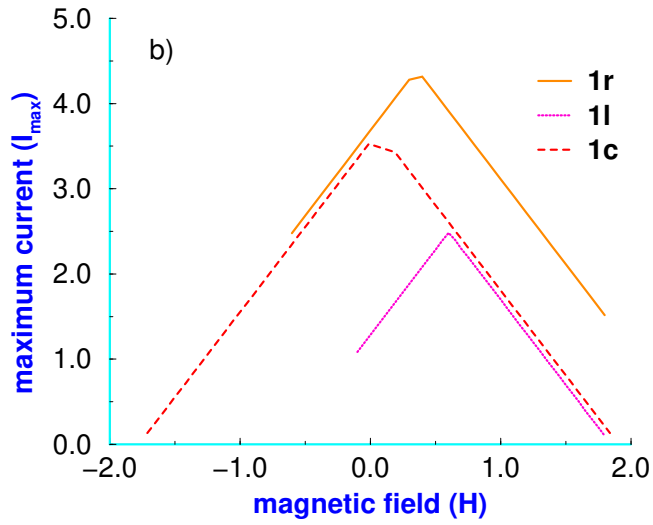
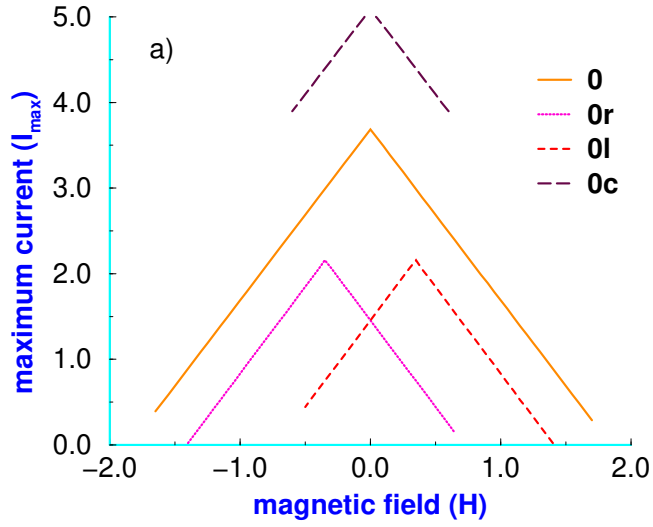


FIG. 11. Critical current I_c , versus the magnetic flux N_f , at their maximum current for the different modes, for a junction of length $\ell = 10$, (a) for the asymmetric defect case, and (b) for the two symmetric pinning centers of length $d = 2$.



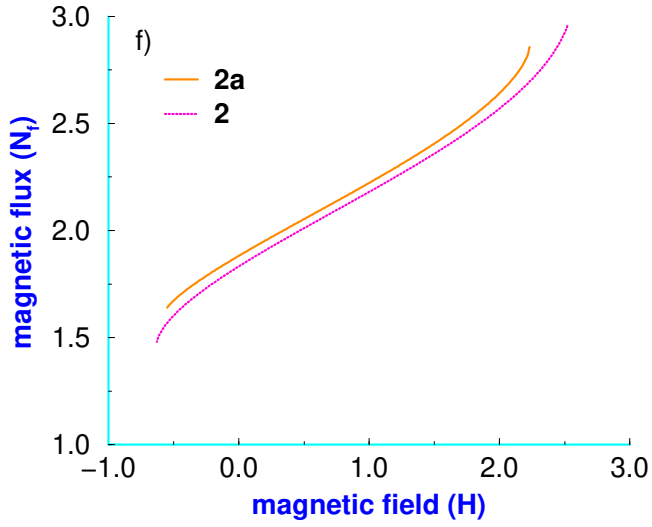


FIG. 12. Critical current I_{max} versus the magnetic field H , for the different modes (a) 0, 0l, 0r, 0c, (b) 1r, 1l, 1c, and (c) 2, 2a, 2b. for a junction of length $\ell = 142$, which contains three symmetric pinning centers of length $d = 2$. The corresponding magnetic flux is presented in (d), (e), (f).

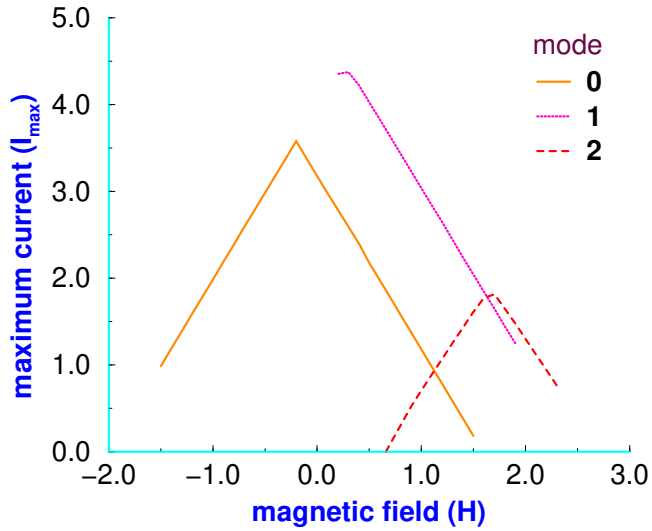


FIG. 13. Inline critical current I_{max} versus the magnetic field H , for the modes 0, 1 and 2, for the junction with an asymmetric defect but smooth variation of the critical current density $x_0 = 7\%$ and $\ell = 2$.

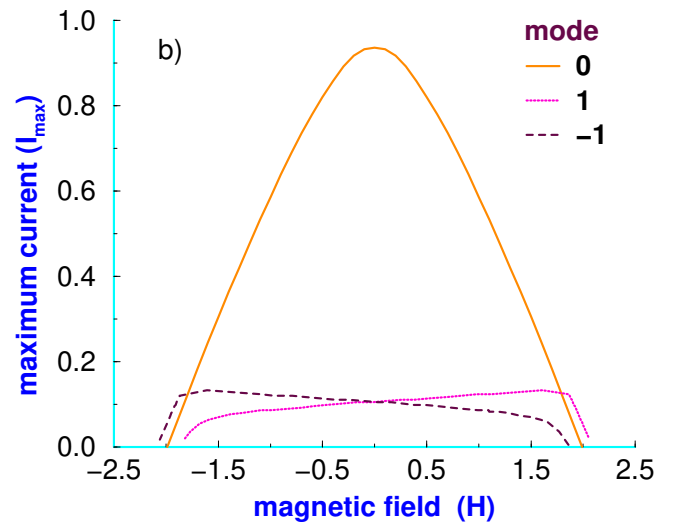
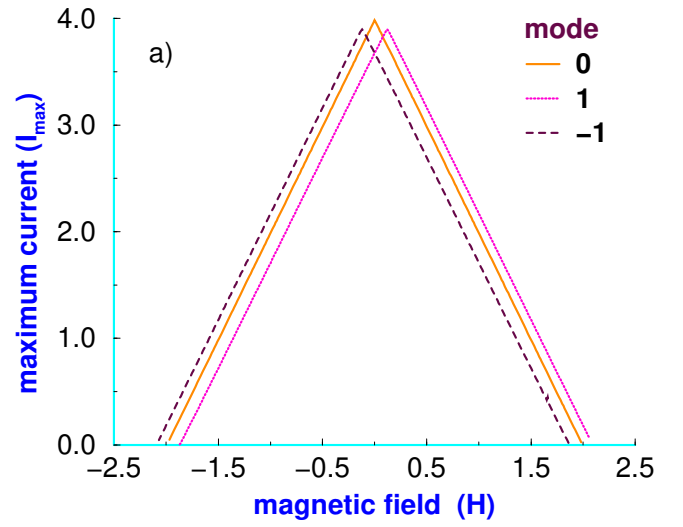


FIG. 14. Critical current I_{max} versus the magnetic field H , for the different modes, for (a) inline current and (b) overlap current, for the junction with a centered defect, and smooth variation of the critical current density.

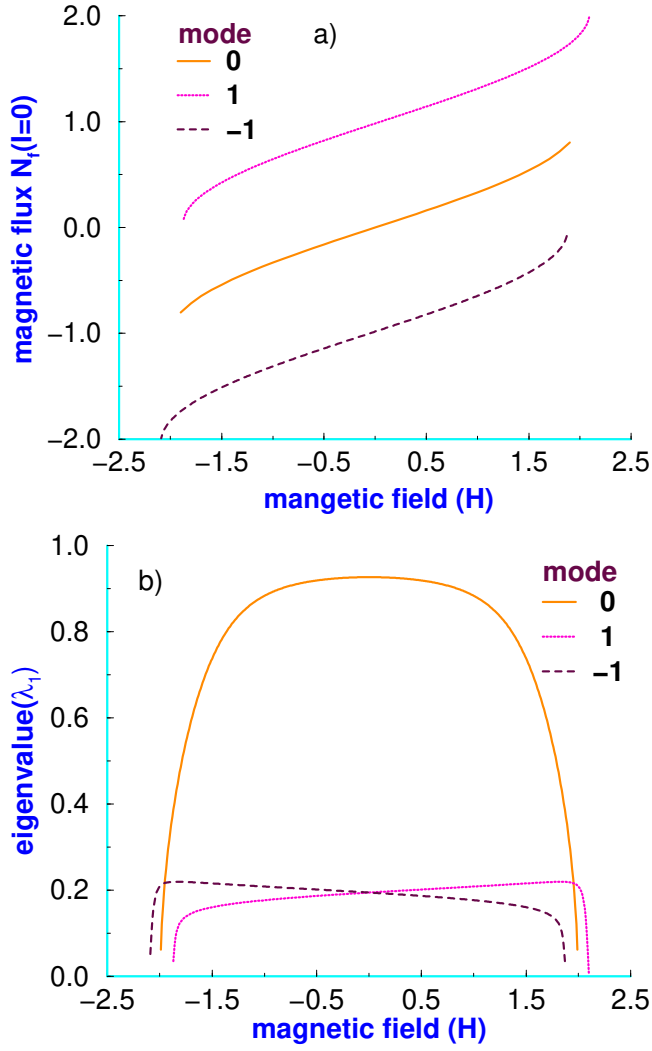


FIG. 15. (a) Magnetic flux at zero current as a function of the external field, for the same type of inhomogeneity as in Fig. 14. (b) The corresponding evolution of the lowest eigenvalue λ_1 for the different modes. At the end of each mode the λ_1 vanishes.

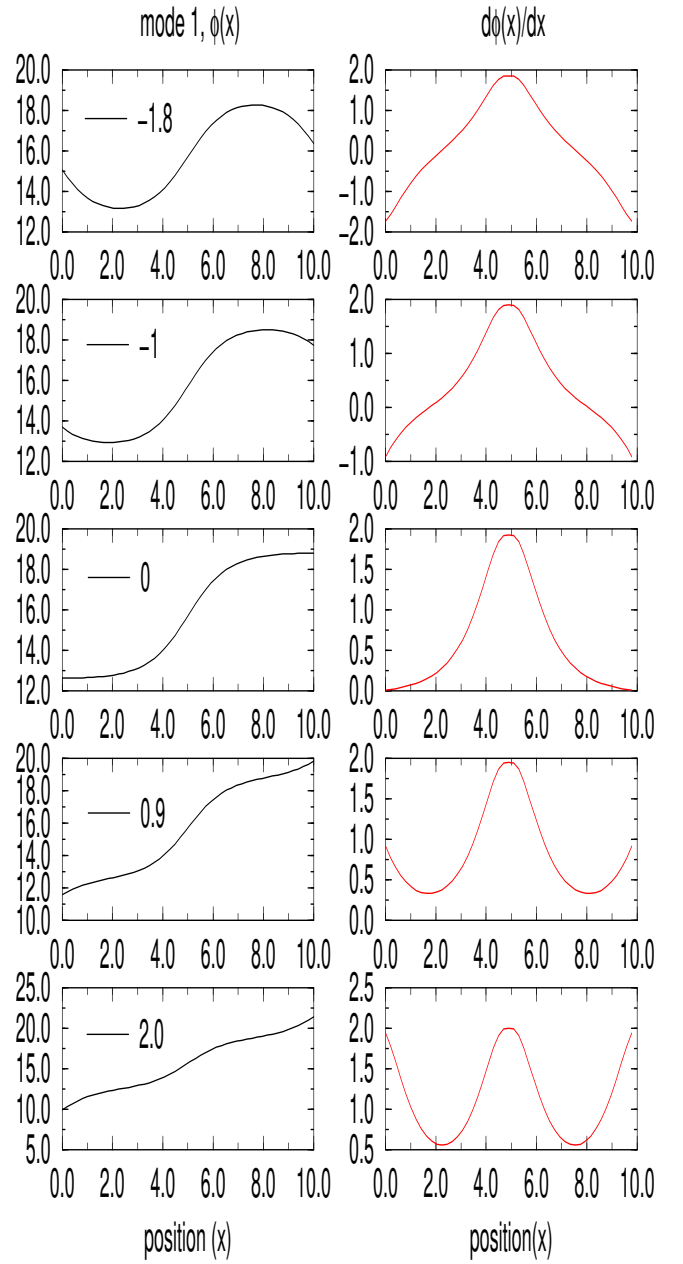


FIG. 16. The evolution of $\phi(x)$ and $\frac{d\phi(x)}{dx}$, for the mode 1, as we change the magnetic field at $I = 0$, for the same type of inhomogeneity as in Fig. 14. Numbers are H values.